Brain Topography (2022) 35:398–415
https://doi.org/10.1007/s10548-022-00899-9

ORIGINAL PAPER

Evaluating Head Models for Cortical Source Localization of the Face-Sensitive N290 Component in Infants

Xiaoxue Fu[1] · **John E. Richards**[1]

Received: 13 December 2021 / Accepted: 9 April 2022 / Published online: 11 May 2022

Abstract

Accurate cortical source localization of event-related potentials (ERPs) requires using realistic head models constructed from the participant's structural magnetic resonance imaging (MRI). A challenge in developmental studies is the limited accessibility of participant-specific MRIs. The present study compared source localization of infants' N290 ERP activities estimated using participant-specific head models with a series of substitute head models. The N290 responses to faces relative to toys were measured in 36 infants aged at 4.5, 7.5, 9, and 12 months. The substitutes were individual-based head models constructed from age-matched MRIs with closely matched ("close") or different ("far") head measures with the participants, age-appropriate average template, and age-inappropriate average templates. The greater source responses to faces than toys at the middle fusiform gyrus (mFG) estimated using participant-specific head models were preserved in individual-based head models, but not average templates. The "close" head models yielded the best fit with the participant-specific head models in source activities at the mFG and across face-processing-related regions of interest (ROIs). The age-appropriate average template showed mixed results, not supporting the stimulus effect but showed topographical distributions across the ROIs like the participant-specific head models. The "close" head models are the most optimal substitute for participant-specific MRIs.

Keywords Source analysis · Event-related potentials · Head models · Infant · Face processing

Introduction

Cortical source analysis of event-related potentials (ERPs) is a neuroimaging analytical tool that facilitates the understanding of functional neural responses across the lifespan. The technique takes the advantage of ERPs that provide temporally sensitive measurement of neural responses time-locked to stimulus presentation. It incorporates structural information from magnetic resonance imaging (MRI) to identify the loci of the neural responses measured at the scalp surface. The selection and construction of head model is a critical step for accurate estimations of the forward model and source localization. The optimal head model for accurate solutions is a realistic head model constructed from the participant's own MRI, which has a close representation of the topographical and electrical properties of the individual's head and brain (Conte and Richards 2021; Vorwerk et al. 2014, 2018). However, MRI data collection might not always be successful considering the challenges of obtaining MRI scans with satisfactory quality in infants and young children. Existing ERP source localization studies (Conte et al. 2020; Guy et al. 2016) and fMRI evidence (Deen et al. 2017) in infants have established that the middle fusiform gyrus (mFG) is a key region underlying infant face processing. The present study compared source localization of infant ERP responses to faces relative to non-face objects using the participants' own head model with several alternative head models.

Cortical source analysis has been implemented to study the brain locations underlying the N290 components in infants. The N290 is a face-sensitive ERP component in infants (Conte et al. 2020; de Haan et al. 2003). It is a developmental precursor of the adult N170 (de Haan et al. 2003; Hoehl and Peykarjou 2012). Cortical source analyses in healthy infants (3 to 12 months) have revealed that the N290 response to faces versus non-face objects was localized in the middle fusiform gyrus (mFG) and the surrounding

Handling Editor: Bin He.

✉ Xiaoxue Fu
xiaoxuef@mailbox.sc.edu

[1] Department of Psychology, University of South Carolina, Columbia, USA

ventral occipitotemporal (VOT) regions (Buiatti et al. 2019; Conte et al. 2020; Guy et al. 2016; Johnson et al. 2005; Xie et al. 2019a, b). The mFG has been found as a neural basis for face processing in studies conducting source analysis of the N170 responses in adults (Richards et al. 2018 for a review), as well as fMRI studies examining neural responses to faces in infants (Deen et al. 2017) and adults (Berman et al. 2010 for a review). Together, cortical source analyses of infants' N290 component have underscored that the adult-like functional organization underlying face processing is at least partially in place during infancy (Powell et al. 2018).

Age-appropriate realistic head models are critical to ensure accurate localization of the neural generator(s) of the N290 activities recorded on the scalp. Accurate source localization, or inverse modeling, strongly depends on an accurate forward model that estimates the electric potential at the scalp electrode locations generated by a source in the brain (Vorwerk et al. 2014, 2018). An accurate forward solution requires specifying the electrode locations on the individual's head and constructing a realistic head model that represents the individual's head geometry (Conte and Richards 2021, 2022; Michel and Brunet 2019; Vorwerk et al. 2014; Vorwerk et al. 2018; Xie and Richards under review).

The requirement for participant-specific MRIs for source analysis poses a challenge for developmental studies due to the difficulties of obtaining MRI scans from infants and young children. The use of adult head models as a substitution for infant or child participant-specific head models increases localization errors. There is extensive brain morphological development during infancy, including increases in GM, WM, and CSF volumes and WM myelination (Gilmore et al. 2011; Makropoulos et al. 2016; Richards and Conte 2020; Richards and Xie 2015). Specifically for studies of the N290 in infants, there is anatomical development in the posterior fusiform gyrus and mFG that is related to functional improvements in face processing (Gomez et al. 2017).

Source localization studies with infants and children have used adult or age-appropriate MRI templates when the participant-specific MRIs were not collected or fully available. Table 1 has listed the type of head models used in the representative developmental studies. Earlier studies that did not collect MRIs from participants used an adult MRI template (e.g., van Leeuwen et al. 2007) or a single-infant MRI template obtained from an age group closely matched with the participants (e.g., Reynolds and Richards 2005). An MRI template constructed from a single infant participant offered a more age-appropriate representation of the participants' head geometry than an adult head model. However, it cannot account for structural variability across participants (Reynolds and Richards 2009). More recent infant studies that did not have participant-specific MRIs adopted age-appropriate average templates constructed from MRIs of a group of age-matched individuals (e.g., Xie et al. 2019a, b), or "close" head models constructed from MRIs of individuals closely matched with each participant's age and head size (e.g., Xie and Richards 2016). Alternatively, infant studies that included MRI data collection used participant-specific MRIs when available, but otherwise used age-appropriate average templates (e.g., Hämäläinen et al. 2011) or "close" MRIs (e.g., Guy et al. 2016). Age-appropriate average templates and "close" head models can be created from study participants (e.g., Hämäläinen et al. 2011), or may be obtained from the publicly available Neurodevelopmental MRI Database (Fillmore et al. 2015a; Richards, in prep; Richards et al. 2015b; Sanchez et al. 2012a, b). The use of age-appropriate average templates or individual-based "close" head models can reduce errors in forward solution and source localization compared to age-inappropriate head models.

One study has compared source solutions obtained from a series of average templates with estimations from participant-specific head models. Guy, Richards, and Roberts (under review) examined source activations of the N290 in response to faces and toys in 12-month infants with high risks of autism spectrum disorder and fragile X syndrome. They constructed study-specific average templates, risk-group-specific average templates from a large MRI database (IBIS; Hazlett et al. 2017), and average templates from 12-month-old, 12-year-old, and adult typically developing individuals, respectively. The risk-group-specific average templates offered the closest fit with participant-specific head models. Specifically, the difference scores between the source activation estimated from the risk-group-specific average templates and the participant-specific head models and were lower compared to the difference scores between other types of average templates and the reference across face-processing-related ROIs. The source solutions obtained from the risk-group-specific average templates also had the highest correlation with the participant-specific head models. It is possible that the group-specific average templates constructed from a large MRI database (IBIS; Hazlett et al. 2017) better represented the between-individual variability in head and brain structures within the high-risk infants (Guy et al. under review).

A conclusion from these studies is that cortical source analysis of EEG/ERP using realistic head models that closely represent the participant-specific structural features (age, head size, and tissue segmentations) would yield more accurate solutions than cortical source analysis with age-inappropriate average templates. The individual-based "close" head models might be the best substitute that can account for individual differences in head geometry (Reynolds and Richards 2009). However, this solution requires accurate participants' head measurements that might not have been collected (Conte and Richards 2022). This begs the question of whether comparable localization accuracy can be achieved with "far" head models that are matched

Table 1 Head models used in representative developmental studies that conducted source localization of EEG/ERP responses

Study	Participant age(s)	Head model(s)
Studies with only EEG/ERP data collection		
Albrecht et al. (2000)	Children: 5 to16 years Adults: 20 to 30 years	An adult head model
van Leeuwen et al. (2007)	2 months	An adult head model
van der Weel and van der Meer (2009)	5 to 11 months	An adult head model
Bernal et al. (2010)	2 years	A template from a 2-year-old
Johnson et al. (2005)	3, 4, and 12 months	A template from a 12-year-old
Reynolds and Richards (2005)	4.5, 6, and 7.5 months	A template from a 6-month-old
Richards (2005)	14 to 20 weeks	A template from a 6-month-old
Buiatti et al. (2019)	Newborns (15 to 96 h)	A template from a 7-week-old
Bathelt et al. (2013)	1.5 to 6 years	Age-matched average templates
Cantiani et al. (2019)	ERP data were collected at 6 months	An age-appropriate average template
Ortiz-Mantilla et al. (2019)	ERP data were collected at 9 months	An age-appropriate (12-month) average template
Thorpe et al. (2016)	12 month, 4 years, and 18 to 21 years	Age-appropriate average templates
Xie, et al. (2019a, b)	6, 8, 10, and 12 months	Age-appropriate average templates
Xie, et al. (2019a, b)	6, 8, 10, and 12 months	Age-appropriate average templates
Xie and Richards (2016)	6, 8, 10, and 12 months	"Close" head models
Xie and Richards (2017)	3 and 4.5 months	"Close" head models
Studies with both EEG/ERP and MRI data collection		
Hämäläinen et al. (2011)	6 months	Subject-specific head models, and an age-matched average template as the substitute
Ortiz-Mantilla et al. (2012)	6 months	Subject-specific head models, and an age-appropriate average template as the substitute
Ortiz-Mantilla et al. (2013)	6 months	Subject-specific head models, and an age-appropriate average template as the substitute
Ortiz-Mantilla et al. (2016)	6 and 12 months	Subject-specific head models, and age-appropriate average templates as substitutes
Conte et al. (2020)	4.5, 6, 7.5, 9, and 12 months	Subject-specific head models, and "close" head models as substitutes
Guy et al. (2016)	4.5, 6, and 7.5 months	Subject-specific head models, and "close" head models as substitutes

"Close" head models were constructed using MRIs close in age and head size with the each of the study participants

EEG electroencephalogram, *ERP* event-related potential, *MRI* magnetic resonance imaging

with individual participants' ages but not head size or age-appropriate average template. Cortical source localization results using substitute MRIs for a participant-specific MRI has not been evaluated.

The present study compared cortical source localization of the N290 ERP response in infants with different head models. The current study used data from Conte et al. (2020) from infants who had source analysis of the N290 ERP based on their own MRI. The primary objective was to compare source activities obtained using participant-specific MRIs with a series of substitute head models. We hypothesized that the source solutions obtained from age-matched individual-based head models and age-appropriate average templates will be like source localization using participant-specific MRIs, and closer than source solutions using head models constructed from age-inappropriate groups. A secondary objective was to confirm the effect of task stimulus (face versus toys) and age on source activities of the N290 at the mFG estimated using realistic head models constructed from infants' participant-specific MRIs, e.g., Conte et al. (2020)'s findings. This study should result in recommendations for selecting an optimal head model for source localization when the participants' own MRI is unavailable.

Method

Participants

Participants were 36 full-term (23 males), typically developing infants aged at 4.5 months, 6 months, 7.5 months, 9 months, or 12 months. Table 2 ("Participant-specific MRIs") displays the demographic information of the study participant. The participants were chosen from a prior study

Table 2 Demographic information of study participant and MRI samples by age group, sex, and data source

Age group	Total *N*	Male *N*	MCBI *N*	BCP *N*	IBIS *N*
Participant-specific MRIs					
4.5 months	6	5	6	0	0
6 months	12	6	12	0	0
7.5 months	11	6	11	0	0
9 months	3	2	3	0	0
12 months	4	4	4	0	0
Potential MRIs					
4.5 months	46	19	5	41	0
6 months	64	34	4	0	60
7.5 months	52	37	3	0	49
9 months	55	22	4	48	3
12 months	103	70	14	0	89
Close MRIs					
4.5 months	6	4	5	1	0
6 months	12	5	4	0	8
7.5 months	11	6	3	0	8
9 months	3	0	3	0	0
12 months	4	3	4	0	0
Far MRIs					
4.5 months	6	3	1	5	0
6 months	12	7	2	0	10
7.5 months	11	10	0	0	11
9 months	3	2	0	3	0
12 months	4	4	2	0	2

MCBI McCausland Center for Brain Imaging, *BCP* Baby Connectome Project, *IBIS* Infant Brain Imaging Study

(Conte et al. 2020) and who had a structural MRI for that study. Participants were primarily Caucasian and of middle socioeconomic status. The study had informed parental consent. The University of South Carolina Institutional Review Board approved data collection.

MRI Data Acquisition

The present study used T1-weighted (T1W) and T2-weighted (T2W) MRI scans from each participant. The MRIs of the participants were collected at the McCausland Center for Brain Imaging (MCBI) in Columbia, SC. Details of the MRI acquisition and processing are described in previous studies (Conte et al. 2020; Guy et al. 2018, 2016; Xie and Richards 2016).

The substitute MRIs (next section) were obtained from the MCBI and open-access databases ($N = 320$). The selected dataset contained 24 MRIs from the MCBI, 9 from the Baby Connectome Project (BCP: Howell et al. 2019), and 39 from the Infant Brain Imaging Study (IBIS: Hazlett et al. 2017). Table 2 ("Potential MRIs") displays the demographic information of the substitute MRIs. The average templates consisted of templates from constructed for the Neurodevelopmental MRI Database (Fillmore et al. 2015a, b; Richards in prep; Richards et al. 2015a, b; Sanchez et al. 2012a, b). An age-appropriate average template, and "age-inappropriate" average templates from 12 months, 12 years, and 20–24 years were used. Details of the MRI acquisition protocols may be found in the open access database sites, and details of the average templates construction in the Neurodevelopmental MRI Database publications. All studies had informed parental consent and institutional review board approval. The data from the open access databases had "Data Use Agreements" and institutional review board approval for use in this study.

Head Model Selection and Construction

We selected substitute MRIs for each participant-specific MRI collected from the participant. The "close" and "far" head models came from the potential substitute MRIs that were age-matched to the participant-specific MRI. We use scalp fiducial locations to measure individuals' head geometry. These locations (the vertex, nasion, inion, and left and right preauricular) are used to anchor EEG net placement and reconstruct scalp electrode positions. The root-mean-square difference between fiducial points of the participant-specific and the candidate head model pairs were minimized for the "close" head model ($M = 24.07$ mm, $SD = 23.18$) and maximized for the "far" head model ($M = 176.50$ mm, $SD = 169.56$). The largest distance between the participant-specific and "close" MRIs was smaller than the smallest distance between the participant-specific and "far" MRIs. The algorithm selects MRIs that have the most similar head measurements as the participant-specific MRIs as the "close" MRIs, whereas the MRIs with the most dissimilar head measurements as the participant-specific MRIs were selected as the "far" MRIs. The additional substitute head models for each participant-specific head model were an age-appropriate average template, 12-month average template (for infants who were not 12 months old), adolescent (12-year) average template, and adult (20–24 years) average template.

The head MRI volume was used to create realistic finite element method (FEM) head models. The MRI volume was segmented into 9 or 10 media types: gray matter (GM), white matter (WM), cerebrospinal fluid (CSF), non-myelinated axons for infants (NMA), dura, skin, skull, air, eyes, and other inside skull material. A tetrahedral mesh was created for the segmented head MRI volume, with each tetrahedron having one value describing its tissue type. Figure 1 displays an example tissue segmentation. Detailed descriptions of the segmentation methods are presented in previous studies (Conte and Richards 2022; Fu and Richards 2021) and

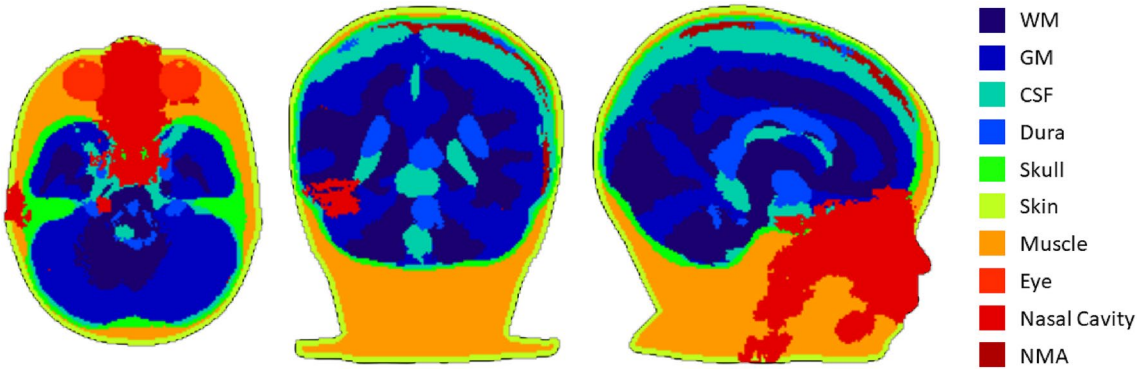

Fig. 1 Multiplanar view of the segmented head MRI volume of a 12-month average template. Infant head models were segmented to 10 tissue types as displayed, and the 12-year and 20–24-year head models were segmented to 9 tissue types (excluding NMA). *WM* white matter, *GM* gray matter, *CSF* cerebrospinal fluid, *NMA* non-myelinated axons

provided in the Supplementary Information. The segmented regions were assembled into a single MRI volume we will refer to as the "segmented head MRI volume". Conductivity value for each segment was set as follow: WM 0.2 S/m, GM 0.33 S/m, CSF 1.79 S/m, dura 0.33 S/M, skull 0.0132 S/m, scalp 0.35 S/m, head muscles 0.35 S/m, eyes 0.5 S/m, nasal cavity 0.0042 S/m, and NMA 0.33 S/m. The conductivity values were used in previous studies with overlapping samples (Conte et al. 2020; Guy et al. 2016).

Virtual Electrode Placement

The electrode locations were estimated on each participant MRI and translated from the participant MRI to the substitute head model type. The placement of the electrodes on the participant MRI and the corresponding substitute MRIs were visually inspected to ensure accuracy. Detailed procedures are described in the Supplementary Information.

Regions of Interest (ROIs)

Anatomical ROIs were defined based on ROIs included in previous studies examining cortical sources of the N290 (Conte and Richards 2022; Conte et al. 2020; Guy et al. 2016). The 15 ROIs included the middle fusiform gyrus (mFG), anterior fusiform gyrus, parahippocampal gyrus, lingual gyrus, medial inferior occipital lobe, lateral inferior occipital lobe, middle inferior occipital lobe, superior occipital lobe, occipital lobe, temporal pole, superior temporal gyrus, middle temporal gyrus, superior temporal sulcus, posterior inferior temporal gyrus, parietal lobe. Figure 2 presents a 3D display of the selected ROIs. Prior findings have shown that the most relevant region associated with the N290 is the mFG outlined in orange (Conte et al. 2020; Gao et al. 2019; Guy et al. 2016). We created a "Ventral Occipital-Temporal (VOT) ROI" (Conte et al. 2020; Gao

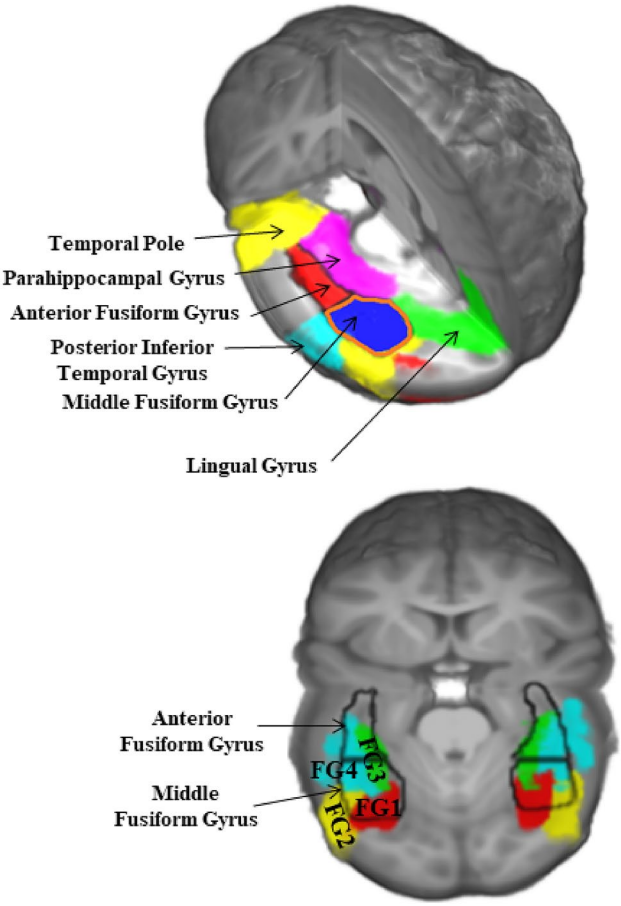

Fig. 2 3D rendering representation of the ventral surface of temporal and occipital lobes on a 12-month-old average template. Top panel shows the main ROIs used to conduct cortical source analysis for the N290 component in response to faces and objects. The most important region is the middle fusiform gyrus (mFG), which is encircled with an orange line. Bottom panel depicts ventral occipital temporal ROIs (FG1-4) described in (Rosenke et al. 2018) and the fusiform gyri transformed into the average 12-month-old template (Color figure online)

et al. 2019; Guy et al. 2016) for some analyses consisting of the mFG, anterior fusiform gyrus, lingual gyrus, parahippocampal gyrus, and temporal pole. The remaining occipital and temporal regions were grouped to form the "Occipital ROI" and "Temporal ROI" for these analyses.

ERP Data Collection and Analysis

The data were from Conte et al. (2020). Infants were presented with pictures of faces and toys while undergoing EEG recording. ERP analysis was conducted to examine the effect of task stimulus type (faces versus toys) on the amplitude of the N290 component. Detailed information on study stimuli, apparatus, procedures, and data analyses were presented in Conte et al. (2020) and summarized in the Supplementary Information.

ERP Source Analysis

Estimations of the forward model and inverse solution were conducted using the Fieldtrip toolbox (Oostenveld et al. 2011) and in-house custom MATLAB scripts (Conte and Richards 2022). We implemented the current density reconstruction (CDR) method for source estimation. The source reconstruction pipeline is detailed in previous studies (Buzzell et al. 2017; Conte and Richards 2022; Conte et al. 2020; Gao et al. 2019; Guy et al. 2016) and the Supplementary Information accompanying those publications (e.g. Richards et al. 2018). We summarized the procedures in the Supplementary Information.

Simulation of N290 Activity from Source

We performed a simulation of the scalp N290 activity to access the accuracy of each head model type for source reconstruction (Conte and Richards 2021). The N290 activity was simulated at each of the 126 electrode locations by multiplying the lead field forward solution by the CDR values at each source volume grid location only in the mFG ROI. The simulated N290 activity was restricted to 12 ms surrounding the peak N290 during stimulus presentation. We quantified the difference between the simulated N290 activity for each head model type and the recorded N290 activity from the participant by computing the relative difference measure (RDM; Güllmar et al. 2010; Meijs et al. 1989; Wolters et al. 2006). The RDM (Eq. 1) quantifies the topographical distribution of the error in the model. A value close to zero indicates that using the given head model to estimate scalp ERP activity yielded similar topographical distribution relative to the ERP activity recorded from the participant (Conte and Richards 2021).

$$RDM = \sqrt{\sum_{i=1}^{n}\left(\frac{sim_x}{\sqrt{\sum_{i=1}^{n}\left(sim_x\right)^2}} - \frac{rec_x}{\sqrt{\sum_{i=1}^{n}\left(rec_x\right)^2}}\right)^2} \quad (1)$$

n denotes electrodes; i is the given electrode; sim_x is the simulated ERP activity using a given head model; and rec_x is the recorded ERP activity from the study participant.

Data Analyses

We first summarized the N290 ERP and source analysis results reported in the previous study (Conte et al. 2020) in the Supplementary Information. Second, we examined the effect of task stimulus and age on the CDR values of the N290 component at the mFG estimated using participant-specific head models. Third, we tested if the substitute head models showed the same stimulus type effect on CDR values in the mFG as the participant-specific head model. Fourth, we compared the topographical distributions of source solutions between head model by examining the CDR values as a function of stimulus type, ROI group, head model, and age group. Fifth, we compared the source reconstruction among different head model types by calculating the relative topographical change of each of the substitute head model from the reference. Next, we conducted between-subject correlations to assess the similarity of CDR values in the mFG between head model types. We also computed within-subject correlations to examine the similarity between the topographical distribution of the CDR values for head model types across all ROIs. Lastly, the head model comparisons of simulated scalp N290 activity were conducted by computing the RDM relative difference score between the substitute and the participant-specific head model. A larger positive difference score indicates that the fit between the recorded ERP activities and simulated ERP activity using the given substitute head model and is worse than the fit between the recorded and simulated ERP data using the participant-specific head models. Data visualizations plotted N290 source activities from -48 to 48 ms around the peak of N290. This is in the range of previous studies (− 40 to 40 ms: Conte et al. 2020; Gao et al. 2019; − 50 to 50 ms: Guy et al. 2016). All formal statistical tests restricted the time window for scalp activity and CDR values to − 12 ms to + 12 ms around the N290 peak, based on data visualization.

Results

Summary of Prior Results (Conte et al. 2020)

Our previous study (Conte et al. 2020) found that the N290 response was greater to faces than toys. The N290 activities were localized in the mFG region. The Supplementary information provides a detailed summary for the findings.

N290 Source Analysis Using Participant-Specific Head Models

We first replicated the previous finding on the stimulus-by-age effect on CDR values of the N290 component estimated using the participant-specific head models. Figure 3 shows the CDR values at the peak of the N290 in the mFG, compared with the values from the temporal pole. The latter that did not show a significant Stimulus effect in Conte et al. (2020). The peak of source response to faces was observable at age 9 months and 12 months. The differences in the CDR values for faces and toys did not occur in the temporal pole in all age groups.

We tested the effect of task stimulus and age group on the CDR values at the mFG of participant-specific head models. A Stimulus (faces and toys) X Age Group (young and old) ANOVA was conducted on the CDR values estimated in the mFG region of the participant-specific head models. We combined age 7.5 months, 9 months, and 12 months to the "old" group based on previous findings (Conte et al. 2020) and examination of the current data. The CDR values surrounding the peak of the N290 (− 12 to + 12 ms) were larger for faces than toys across both age groups, F (1, 32) = 5.64, $p = 0.02$. The Stimulus X Age Group interaction was not significant, $p = 0.26$. Although the interaction was not significant, Table 3 contains the *Scheffé*-corrected simple effects to assess the effect of Stimulus in the young and old infant group separately. The CDR to faces was larger than toys for the older age group but not for the younger age group.

Table 3 *Scheffé*-controlled post-hoc tests for the Stimulus X Age Group interaction on the CDR values in the mFG estimated using the subject-specific head models

Age group (months)	$F_{Scheffé}$ for stimulus	$F_{Scheffé}$ (1, 32), $p = 0.05$	$F_{Scheffé}$ (1, 32), $p = 0.01$	η^2
4.5, 6	0.70	4.14	7.49	0.02
7.5, 9, 12	**6.58**	**4.14**	**7.49**	**0.17**

$F_{Scheffé}$ represents the computed F value for the post-hoc groups or the *Scheffé* criterion for the simple effects tests. The $F_{Scheffé}$ computation is defined in http://www.utstat.toronto.edu/~brunner/oldclass/429f07/text/2007F_Ch6.pdf. The older infant group (bolded) showed significant task stimulus effect

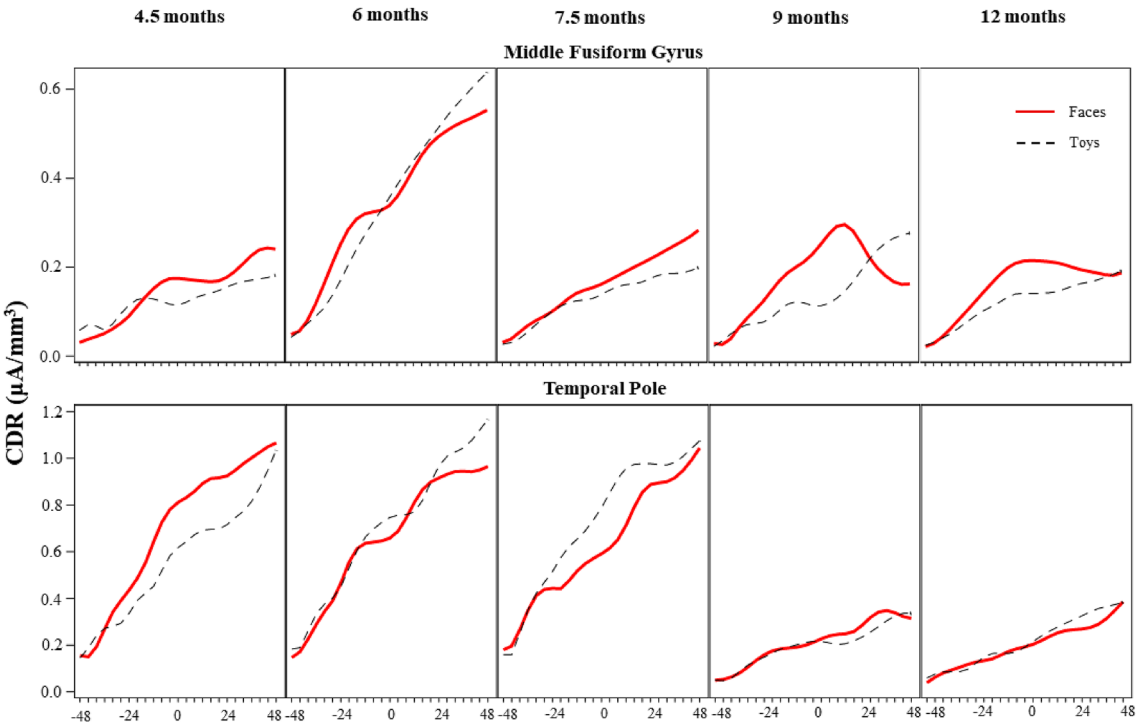

Fig. 3 Line graphs of the CDR values around the peak of N290 (from − 48 to 48 ms) in the middle fusiform gyrus (mFG) and temporal pole by task stimulus type and age

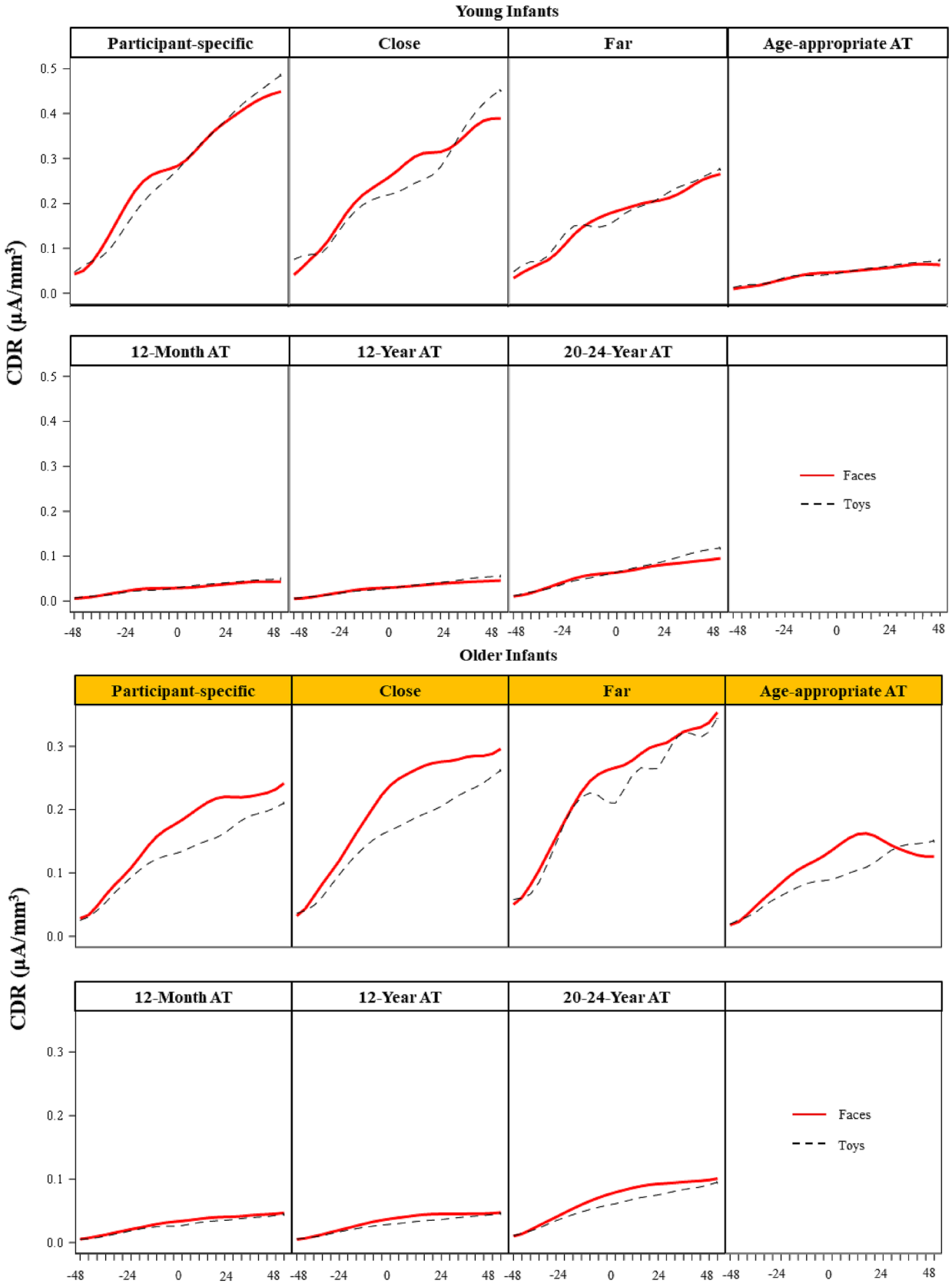
Young Infants
Participant-specific
Close
Far
Age-appropriate AT
12-Month AT
12-Year AT
20-24-Year AT
CDR (µA/mm³)
Faces
Toys
Older Infants
Participant-specific
Close
Far
Age-appropriate AT
12-Month AT
12-Year AT
20-24-Year AT
CDR (µA/mm³)
Faces
Toys

◂**Fig. 4** CDR values in response to faces and toys at the middle fusiform gyrus around the peak of N290 (from − 48 to 48 ms) by head model types separately for young (4.5 months and 6 months) and older infants (7.5 months, 9 months, 12 months). Greater source activities in response to faces than toys around the peak of N290 can be observed in the participant-specific, "close", "far", and age-appropriate average template highlighted in yellow. *AT* average template (Color figure online)

Head Model Comparison

We compared the source activations in response to faces and toys across head model types. First, we investigated whether the stimulus type effect on the CDR values at the mFG was maintained when using the substitute head models. A Stimulus × Head Model (participant-specific, "close", "far", age-appropriate template, 12-months average template, 12-years average template, adult average template) × Age Group ANOVA was done on the averaged CDR amplitudes around the peak of the N290 (− 12 ms to 12 ms) in the mFG. There was a significant main effect of Stimulus, F (1, 34) = 7.66, $p = 0.009$, and Head Model, F (6, 194) = 25.75, $p < 0.001$, and an interaction between Stimulus and Head Model, F (6, 192) = 3.89, $p = 0.001$. There were no significant effects involving the age groups, p's > 0.07. Figure 4 shows the CDR amplitudes at the mFG for faces and toys around the peak of N290 by head model types separately for young and older infants. Figure 5 presents the mean CDR values at the mFG averaged across time points around the peak of N290 by stimulus, head model, and age group. The CDR to faces was larger than to toys primarily for the participant-specific, "close", "far", and age-appropriate average template. This effect appears to be larger in the older group although the effects involving age were not significant. Table 4 contains the results of a post-hoc comparisons of mean CDR values comparing faces versus toys for each head model type corrected with *Scheffé*'s test. The CDR values at the mFG were greater for faces than for toys only for the participant-specific, "close", and "far" head models.

We included CDR values from multiple anatomical ROIs to compare the differences in the topographical distribution of CDR values for faces and toys between head models. We grouped the individual ROIs into three ROI groups: the Ventral Occipital Temporal (VOT) regions encompassed the mFG, anterior fusiform gyrus, lingual gyrus, parahippocampal gyrus, and temporal pole (Conte et al. 2020; Gao et al. 2019; Guy et al. 2016). The "Occipital" and "Temporal" groups included the remaining occipital and temporal regions. The mean CDR values across time points around the peak of N290 (from − 12 to 12 ms) were analyzed in a Stimulus × ROI (VOT, Occipital, Temporal) × Head Model × Age Group ANOVA. There was a significant main effect of ROI group, F (2, 68) = 68.82, $p < 0.001$, and head model, F (6, 200) = 57.11, $p < 0.001$. The ROI-group-by-head-model interaction effect was also significant, F (12, 400) = 18.59, $p < 0.001$. The effects involving Stimulus were not significant, p's > 0.15. Figure 6 displays the mean CDR values as a function of ROI group (VOT, Occipital, and Temporal) and head model type. Table 5 contains the results of a post-hoc comparisons of mean CDR values for the ROI groups for each head model type corrected with *Scheffé*'s test. The post-hoc test compared the CDR value from the VOT to the mean of the Occipital and Temporal ROIs. The CDR activity at the VOT region was greater than the Occipital and Temporal mean CDR for the participant-specific, "close","far", and age-appropriate average template, but did not differ significantly for the other head model types.

We compared the source activations for faces and toys across head model types by computing the absolute difference of CDR values between the participant-specific head model and each of the substitute head models (Eq. 2). This was done using the CDR values at each ROI for each head model to account for differences in source voxel locations in different head models. A small value indicates a smaller difference in between the source activation in response to task stimuli estimated using the given substitute and participant-specific head model. Figure 7 presents ogive curves that describe the cumulative frequency distribution of the CDR absolute difference values separately for all ROIs, the VOT regions, and the mFG ROI. The CDR absolute difference scores showed similar distributions for the "close" and "far" head models for all three figures. Specifically, the absolute difference scores were clustered at smaller values. The distributions were noticeably different for the four types of average templates in the VOT region. The CDR absolute difference scores were more evenly distributed (i.e., more larger values) for these average templates compared to the individual-based head models. The differences in the distribution among the "close", "far", age-appropriate average template, and adult average template were less discernible in the figures for all ROIs and the mFG.

$$Absolute\ Difference\ Score = \left| CDR_{sub} - CDR_{ref} \right| \quad (2)$$

The distribution of source activations to faces and toys for the head model types was compared in 3D rendered volumes of the CDR activity. Figure 8 presents the 3D rendering of the CDR values around the peak of N290 (− 12 ms to 12 ms) as a function of stimulus type and head model type (participant-specific, "close", "far", and age-appropriate average template) for an example infant. The mFG is outlined to emphasize this ROI. The source activation was greater in the mFG for faces than toys in all head mode. The "close" head model had the most similar distribution of source activities at the mFG with the participant-specific head model. The

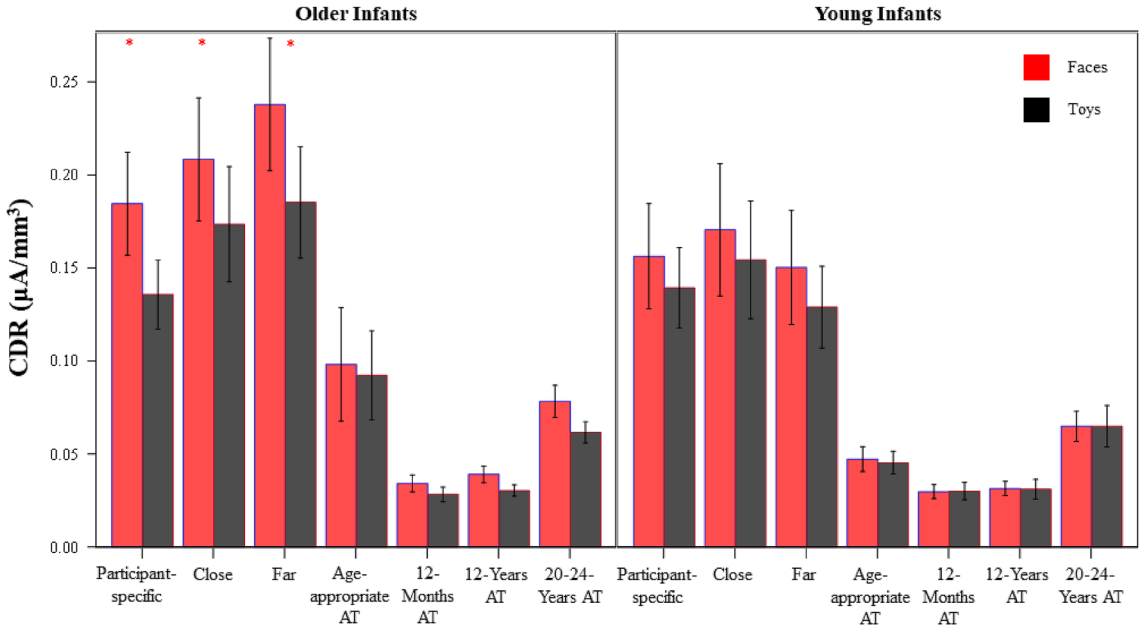

Fig. 5 Mean CDR values in response to faces and toys at the middle fusiform gyrus across time points around the peak of N290 (from − 12 to 12 ms) by head model types separately for young (4.5 months and 6 months) and older infants (7.5 months, 9 months, 12 months). The asterisk signs denote significant differences in CDR values for faces versus toys. *AT* average template

age-appropriate average template also displayed CDR activities for faces in the mFG region as in the participant-specific head model.

Correlation Analyses

We used Pearson correlation analyses to compare the source solutions estimated using different head models. First, between-subject correlations were computed to examine the associations of CDR values around the peak of N290 (from − 12 to + 12 ms) for faces and toys at the mFG. This represents the individual differences in the mFG CDR values for the head models across individuals. Figure 9A shows the results of between-subject correlations when comparing mean CDR values at the mFG estimated using the different head modes with the participant-specific and adult average template as the reference. The mean CDR values at the mFG estimated using the participant-specific head model were positively correlated with the two individual-based head models, the 12-month, 12-year, and adult average templates, p's < 0.001. In contrast, the correlation between the participant-specific and age-appropriate average template was not significant, $p = 0.59$.

Second, within-subject correlations were conducted to compare the similarity between head model types in the spatial distribution of CDR values for faces and toys from all ROIs. We computed Pearson correlations between all ROI pairs for everyone. The r values were then averaged across participants by head model types. This analysis represents the spatial distribution of the CDR across ROIs within an individual for different head models. Figure 9B displays the results of within-subject correlations across all ROIs when the participant-specific head model and adult average template were used as the reference. The mean CDR values estimated using participant-specific head models had stronger correlations with the "close", age-appropriate average template, and 12-month average template but weaker correlation with 12-year and adult average template. In contrast, the source activity estimated using the adult average template was strongly correlated with the 12-month

Table 4 *Scheffé*-controlled post-hoc tests for the Stimulus X Head Model interaction on the CDR values in the mFG

Head model	$F_{Scheffé}$ for stimulus	$F_{Scheffé}$ (6, 192), p = 0.05	$F_{Scheffé}$ (6, 192), p = 0.01	η^2
Participant-specific	**22.16**	**12.87**	**17.38**	**0.103**
Close	**20.48**	**12.87**	**17.38**	**0.096**
Far	**26.43**	**12.87**	**17.38**	**0.121**
Age-appropriate	2.16	12.87	17.38	0.011
12-month average	0.1	12.87	17.38	0.001
12-year average	0.41	12.87	17.38	0.002
Adult average	1.41	12.87	17.38	0.007

$F_{Scheffé}$ represents the computed F value for the post-hoc groups or the *Scheffé* criterion for the simple effects tests. The effect of Stimulus was significant for head model types highlighted in bold

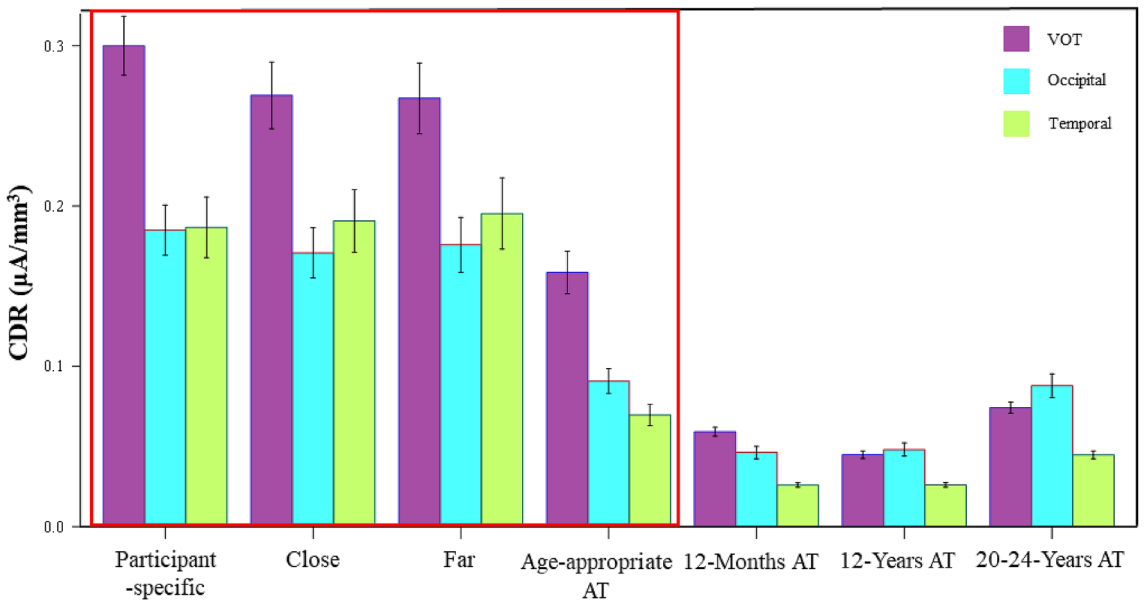

Fig. 6 Mean CDR values across time points surrounding the peak of N290 (from − 12 to 12 ms) as a function of ROI group (Ventral Occipital Temporal, Occipital, and Temporal regions) and head model type. Head model types that showed significant between-ROI-group differences are highlighted in red. *AT* average template (Color figure online)

and 12-year average template but less correlated with the individual-based head models.

Simulated N290 Activity from Source on the Scalp

The distribution of source activations for the head model types was examined by simulating EEG/ERP activity on the scalp by a forward model computation of the CDR in the mFG to the scalp. This analysis used the CDR value in the mFG and projected the scalp activity resulting from that CDR. We compared the projected and the actual EEG/ERP values. Figure 10A displays 3D plots of the scalp distribution of the recorded N290 activity around the peak in response to faces and toys and the scalp distributions of simulated N290 activity using each head model type for an example infant, and using the mFG CDR. The scalp distribution was the same between the recorded data from the participant and the simulated N290 activity from the participant-specific head model. The distribution pattern was similar for the "close", "far", age-appropriate average template, and 12-month average template, but noticeably different for the child and adult average template. Figure 10B presents the RDM difference score between the given head model and the participant-specific head model by head model types using the CDR for the whole head, mFG, VOT, Occipital, and Temporal regions. The difference in the topographical distribution of the simulated N290 activity using "close" and participant-specific head model was small for in the mFG face processing region, the Occipital region, and across the whole head. The age-appropriate average template showed a considerable difference to the participant-specific head model in the mFG but exhibited a smaller difference across the whole head and in the Occipital and Temporal regions. The adult average template did not show a close fit with the participant-specific head model across the whole head or in individual ROIs.

Table 5 *Scheffé*-controlled post-hoc tests for the ROI Group X Head Model interaction on the CDR values in the VOT, Occipital, and Temporal ROIs

Head model	$F_{Scheffé}$ for ROI	$F_{Scheffé}$ (12, 400), p = 0.05	$F_{Scheffé}$ (12, 400), p = 0.01	η^2
Participant-specific	**77.42**	**21.31**	**26.75**	**0.162**
Close	**46.47**	**21.31**	**26.75**	**0.104**
Far	**26.43**	**21.31**	**26.75**	**0.089**
Age-appropriate	**39.52**	**21.31**	**26.75**	**0.085**
12-month average	2.87	21.31	26.75	0.007
12-year average	0.36	21.31	26.75	0.001
Adult average	0.36	21.31	26.75	0.001

$F_{Scheffé}$ represents the computed F value for the post hoc groups or the *Scheffé* criterion for the simple effects tests, comparing the VOT to the mean of the Occipital and Temporal ROIs. The head model types that displayed significant ROI-group-differences are bolded

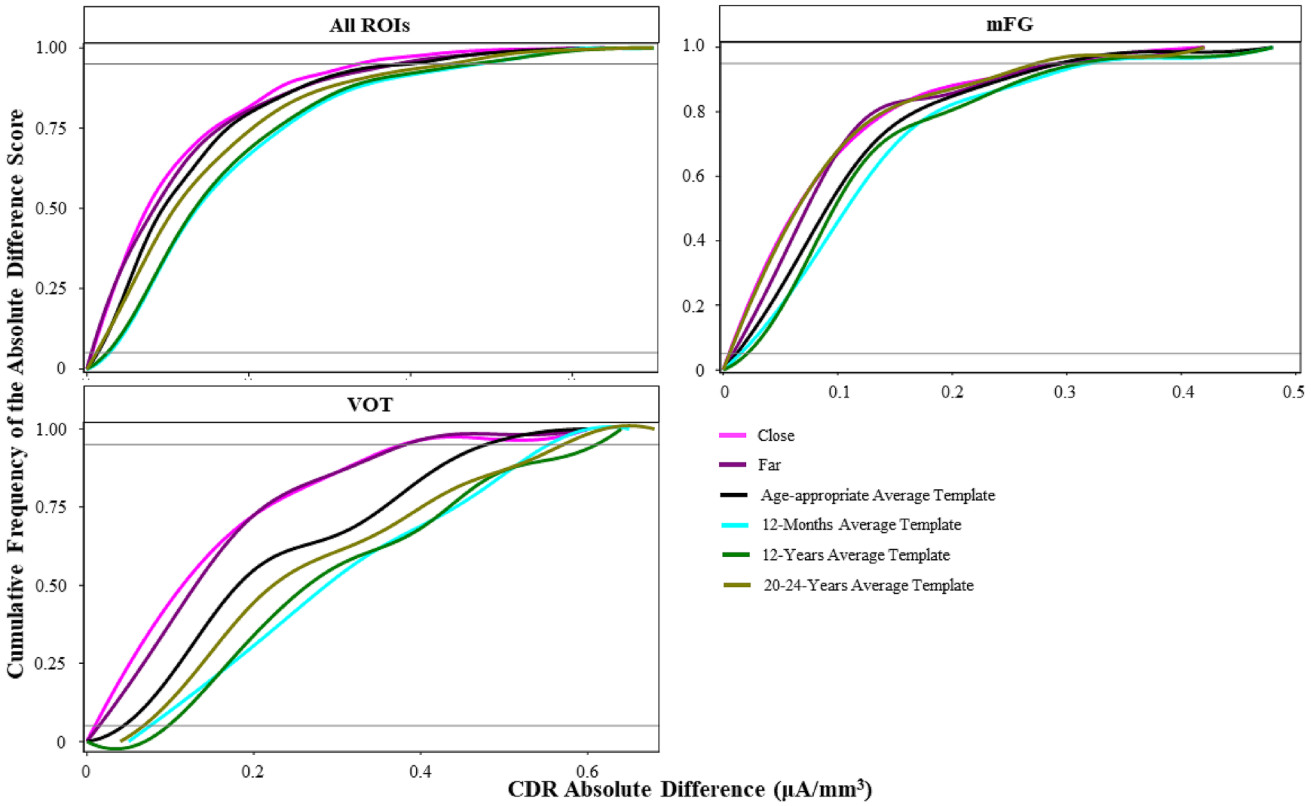

Fig. 7 Cumulative relative frequency of the CDR absolute difference values between the subject-specific and each of the "substitute" head models. The CDR absolute difference values were presented separately for all ROIs, the Ventral Occipital Temporal (VOT) region, and the middle fusiform gyrus (mFG). The horizontal grey lines represent 5% and 95% of cumulative relative frequency

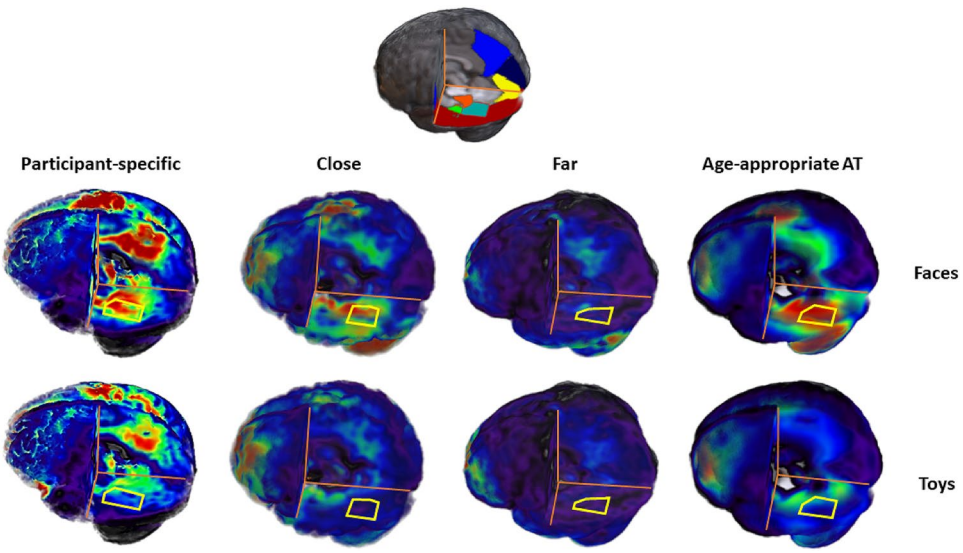

Fig. 8 Three-dimensional renderings of the CDR values around the peak of the N290 component (− 12 ms to 12 ms) by task stimulus type and head model type for an example infant (7.5 months old). The middle fusiform gyrus (mFG) is displayed as the teal region in the head model. The mFG in each head model is outlined in yellow. Additional plots for the 12-month, 12-year, and adult average templates are displayed in Supplementary Fig. 7. *AT* average template (Color figure online)

Discussion

The primary objective of the study was to compare CDR values estimated using realistic head models constructed from infants' participant-specific MRIs with a series of substitute head models. We used FEM models constructed using a participant's own MRI, an MRI from a different participant at the same age with head size "close" or "far" in distance, an age-appropriate average template, and three

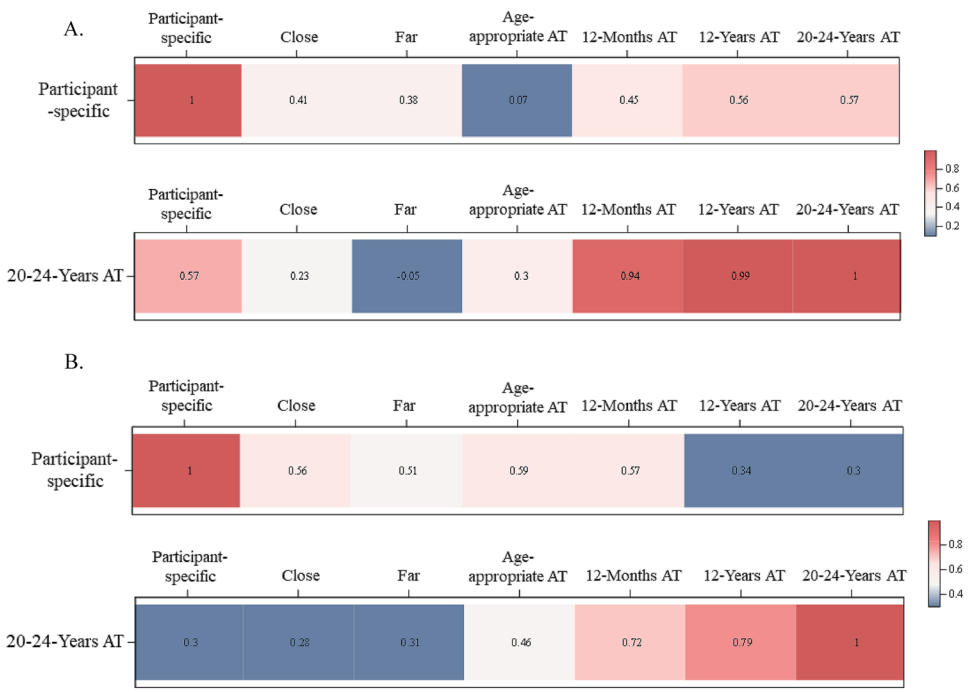

Fig. 9 Correlation results of mean CDR values across time points around the peak of N290 (from − 12 to 12 ms) for faces and toys with the participant-specific and 20–24-year average template as the references. **A** Between-subject correlations of mean CDR values at the middle fusiform gyrus. **B** Averaged within-subject correlations of mean CDR values for all regions of interest (ROIs)

age-inappropriate average templates. The participant-specific, close, and far head models result in similar stimulus effects in the mFG ROI. The "close", "far", and age-appropriate average template preserved the participant-specific topographical distribution of source activities. This was characterized by enhanced activations to faces in the VOT ROI, and higher within-subject correlations with the participant-specific MRI FEM models. The three age-inappropriate average templates, 12 months, 12 years, and adults, did not show the same significant stimulus effects in the mFG, did not preserve the topographical distribution of effects across ROIs within a subject, and showed the lowest correlations with the participant-specific MRI FEM models. The present findings underscored the importance of using age-matched head models for source localization in infants. The "close" head models provide an optimal fit with the participant-specific head models.

The current findings are consistent with existing evidence suggesting that substitute head models that closely represent participants' individual variability in head geometry yield the best fit with participant-specific head models. Guy et al. (under review) showed that the risk-group-specific average template constructed from a large MRI database yielded source activation results more like the participant-specific head models compared to the study-specific and age-appropriate average templates. Furthermore, source analysis using participant-specific head models and risk-group-specific average template as the substitute confirmed that the differentiation of source response to faces versus toys was greatest at the mFG across all participants. The analysis also revealed group differences in the pattern of source activations across face-processing-related ROIs in response to faces and toys. The present study extended from Guy et al. (under review) by including age-matched, individual-based substitute head models. We showed that head models that were more representative of individual differences in head structures provided better fit to the participant-specific head models than the age-appropriate average templates.

Cortical source localization studies of infant EEG/ERP responses to faces have used a single-infant MRI template, age-appropriate average templates, and "close" head models as substitute head models. Johnson et al. (2005) used a 2-year-old MRI template to localize the cortical generator of the N290 ERP to faces. They localized N290 responses to upright and inverted faces to the fusiform gyrus, the right superior temporal sulcus and surrounding temporal regions. Xie et al. (2019a, b) used age-appropriate average templates. They localized N290 responses to emotional faces to the fusiform gyrus and the inferior occipital gyrus. Our findings with individual-based head models were consistent with previous studies that used both participant-specific head models and "close" head models as substitutes (Conte et al. 2020; Guy et al. 2016). The findings collectively suggest that the N290 activities are localized in the VOT network, with the mFG shows the greatest response to faces relative to non-face objects.

Our findings show that the "close" head models preserved the increased source response to faces relative to toys at the mFG (Fig. 5). They produced similar topographical distributions as the participant-specific head models in source

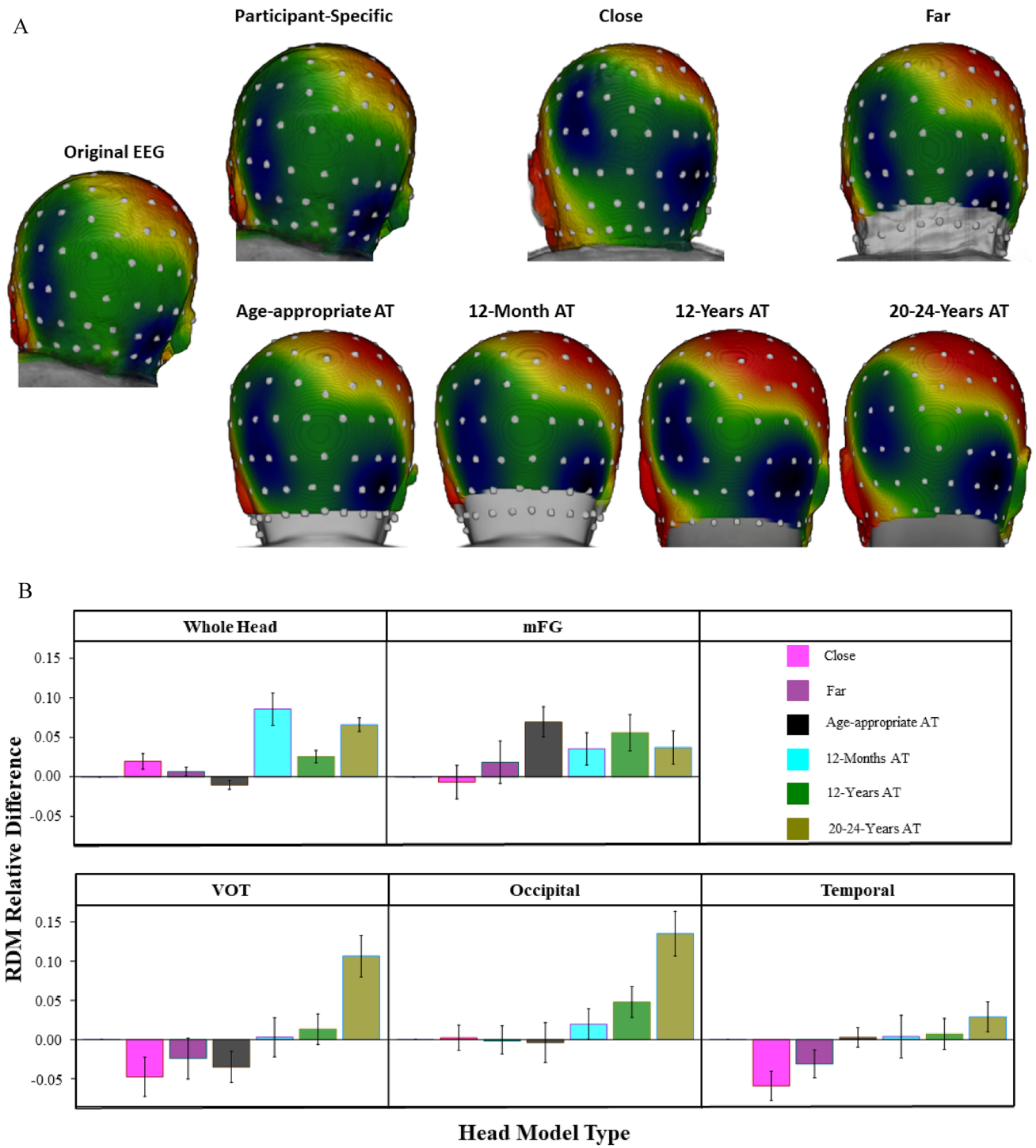

Fig. 10 The simulated N290 surrounding the peak (− 12 ms to + 12 ms) in response to faces and toys as a function of head model. **A** Three-dimensional plots of the scalp distribution of the recorded N290 activity around the peak in response to faces and toys and the scalp distributions of simulated N290 activity by head model type for an example infant (7.5 months old). **B** The difference between RDM for the given head model and the participant-specific head model by head model types for the whole head, the middle fusiform gyrus (mFG), the Ventral Occipital Temporal (VOT), Occipital, and Temporal regions. *AT* average template

activations (Fig. 7) and simulated scalp N290 activities across the whole brain (Fig. 10). We speculate that there are several reasons that the "close" head model minimized source localization errors. First, they may provide a better approximation of electrode placement positions. Our individualized approach for electrode co-registration accounts

for individual differences in head geometry, thus constrains source locations to a realistic topography for the individual (Reynolds and Richards 2009; Richards et al. 2015a; Wang and Gotman 2001). A partial reason for the similar effects for the participants-specific and the "close" head model may be due to the electrodes falling on the same scalp locations and similar cortical development related to head size. Second, the "close" head models may provide a better spatial representation of the tissue types in the head. The realistic head models constructed from the age- and head-size-matched MRIs likely provide developmentally appropriate descriptions of head and brain tissues. Evidence has shown that the inclusion of CSF and GM/WM distinction in head models significantly improved accuracy in forward modeling (Azizollahi et al. 2016) and source localization (Azizollahi et al. 2020; Conte and Richards 2021). Our FEM models accurately model both superficial CSF and intraventricular CSF and thus improve source localization accuracy in infants (Conte and Richards 2021). The similar age and head size likely produced a similar CSF profile and thus similar CDR results. Third, the "close" head models may provide a better approximation of the individual's head geometry. The "close" head models may minimize differences in head size, tissue geometry, and electrode locations with the infant's participant-specific head model can successfully maintain the accuracy of source localization.

The use of average templates is less optimal than individual-based head models for source localization. Average templates and the associated source space may not account for individual differences in anatomical structures, electrical properties of the head tissues, and locations of the ROI (Conte and Richards 2022; Reynolds and Richards 2009). For example, the low between-subject correlation of mean CDR values at the mFG shown in Fig. 9A may be driven by large between-individual variations in the fit between participant-specific head models and the age-appropriate average template. Average templates may also have smoothed out or misplaced the source activities that occurred in the relatively small mFG ROI (Fig. 8). It is possible that the stimulus effect on source activities were localized to a different region within the VOT network due to differences in electrode placement between the individual and the average templates.

Neither the age-appropriate nor age-inappropriate (12-month, 12-year, and adult) average templates yielded satisfactory fit with source solutions from the participant-specific head models compared to individual-based "close" head models. The age-appropriate average templates produced source activities and simulated N290 scalp activities with comparable topographical distributions as the individual-based head models across ROIs (Figs. 6, 7, 9B, and 10). However, the use of age-appropriate average template failed to detect the stimulus effect on source activations at the mFG as estimated with individual-based head models (Fig. 5). The age-inappropriate average templates yielded a worse fit the participant-specific head models compared to age-matched head models. The age-inappropriate average templates disguised the stimulus effect at the key face area (Figs. 4, 5). They altered the signal topography estimated using infants' participant-specific head models (Figs. 7, 9B). Differences in head size and brain structural characteristics between the participant-specific head models and the age-inappropriate average templates contribute to the errors in forward model estimations and source localization. Child and adult head models have greater scalp-to-cortex distances than infant head models (Beauchamp et al. 2011; Fu and Richards 2021). Some of structural difference can be attributed to increased skull thickness (Hansman 1966) and CSF volume (Makropoulos et al. 2016) during development. There is also extensive growth in the GM, WM, and global brain volume (Gilmore et al. 2011; Makropoulos et al. 2016; Richards and Conte 2020; Richards and Xie 2015). Inaccurate representations of the anatomical geometry of brain tissue segments can lead to estimation errors of forward models (Cho et al. 2015; Vorwerk et al. 2014, 2018), which may have happened with the age-inappropriate average templates. The use of child and adult head models may lead to exclusion or misrepresentation of intraventricular CSF in infant head models (Conte and Richards 2021). Together, the present studies have demonstrated that it is less optimal to use average templates compared to "close" head models, and it is inappropriate to use age-inappropriate average templates for source localization in infants.

Our findings underscored the benefits of using individual-based "close" head models when the participant-specific head models are unavailable. In the case that the participant's head measurements were not collected, our findings indicate that a random selection of an individual head model with the same age as the study participant or an age-appropriate average template would be superior to using age-inappropriate average template. If researchers do not have access to age-matched individual head models, we recommend researchers use age-appropriate or study-specific average templates (Conte and Richards 2022; Guy et al. under review).

A limitation of the current study is that we did not set age-specific conductivity values for the tissue segments. Infants have higher skull conductivity than adults (Odabaee et al. 2014). This can be attributed to thinner skull the presence of fontanels and skull sutures in infants (Hansman 1966). Some studies in infants and pediatric samples have adopted a higher skull conductivity value than the present study (e.g., Hämäläinen et al. 2011; Lai et al. 2005), although these studies used spherical shell head models. There are also age-related changes in GM and WM conductivity during myelination (Azizollahi et al. 2016). Inaccurate specification of the skull conductivity (Lew et al. 2013) and

the differential conductivity of GM and WM (Azizollahi et al. 2016) can negatively affect the accuracy of forward modeling and source localization. Future research is needed to identify the age-specific ranges of conductivity values for different tissue types.

In summary, the present study built from existing research that has identified the mFG and the surrounding VOT network as the cortical generator of enhanced N290 responses to faces relative to non-face objects in infants. We compared source activities in response to the task stimuli at the mFG and face-processing-related ROIs estimated using participant-specific ROIs and a series of alternative head models. The "close" head models yielded the best fit with the participant-specific head models in source activities at the mFG and across face-processing-related regions of interest. The age-appropriate average template showed mixed results, not supporting the full significance tests for the stimulus effect but showed topographical distributions across the ROIs like the participant-specific model. The present findings indicated that the "close" head models are the most optimal substitute when participant-specific MRIs were not available.

Supplementary Information The online version contains supplementary material available at https://doi.org/10.1007/s10548-022-00899-9.

Acknowledgements This research was supported by grants from the National Institute of Child Health and Human Development (NICHD-R01-HD18942, NICHD-R37-HD18942, NIHCD-R03-HD091464) to J.E. Richards.

Data Availability The age-specific individual MRIs and average templates can be accessed from the "Neurodevelopmental MRI Database". The Database is available online: http://jerlab.psych.sc.edu/NeurodevelopmentalMRIDatabase/ for information and https://www.nitrc.org/projects/neurodevdata/ for access. Details on the online access are provided in Richards et al. (2015b). The codes that support the findings of this study are available from the corresponding author, XF, upon request.

References

Albrecht R, Suchodoletz W, Uwer R (2000) The development of auditory evoked dipole source activity from childhood to adulthood. Clin Neurophysiol 111(12):2268–2276

Azizollahi H, Aarabi A, Wallois F (2016) Effects of uncertainty in head tissue conductivity and complexity on EEG forward modeling in neonates. Hum Brain Mapp 37(10):3604–3622. https://doi.org/10.1002/hbm.23263

Azizollahi H, Aarabi A, Wallois F (2020) Effect of structural complexities in head modeling on the accuracy of EEG source localization in neonates. J Neural Eng 17(5):056004. https://doi.org/10.1088/1741-2552/abb994

Bathelt J, O'Reilly H, Clayden JD, Cross JH, de Haan M (2013) Functional brain network organisation of children between 2 and 5years derived from reconstructed activity of cortical sources of high-density EEG recordings. Neuroimage 82:595–604. https://doi.org/10.1016/j.neuroimage.2013.06.003

Beauchamp MS, Beurlot MR, Fava E, Nath AR, Parikh NA, Saad ZS, Oghalai JS (2011) The developmental trajectory of brain-scalp distance from birth through childhood: implications for functional neuroimaging. PLoS ONE 6(9):e24981. https://doi.org/10.1371/journal.pone.0024981

Berman MG, Park J, Gonzalez R, Polk TA, Gehrke A, Knaffla S, Jonides J (2010) Evaluating functional localizers: the case of the FFA. Neuroimage 50(1):56–71

Bernal S, Dehaene-Lambertz G, Millotte S, Christophe A (2010) Two-year-olds compute syntactic structure on-line. Dev Sci 13(1):69–76. https://doi.org/10.1111/j.1467-7687.2009.00865.x

Buiatti M, Di Giorgio E, Piazza M, Polloni C, Menna G, Taddei F, Vallortigara G (2019) Cortical route for facelike pattern processing in human newborns. Proc Natl Acad Sci USA 116(10):4625–4630

Buzzell GA, Richards JE, White LK, Barker TV, Pine DS, Fox NA (2017) Development of the error-monitoring system from ages 9–35: Unique insight provided by MRI-constrained source localization of EEG. Neuroimage 157:13–26

Cantiani C, Ortiz-Mantilla S, Riva V, Piazza C, Bettoni R, Musacchia G, Benasich AA (2019) Reduced left-lateralized pattern of event-related EEG oscillations in infants at familial risk for language and learning impairment. Neuroimage 22:101778. https://doi.org/10.1016/j.nicl.2019.101778

Cho J-H, Vorwerk J, Wolters CH, Knösche TR (2015) Influence of the head model on EEG and MEG source connectivity analyses. Neuroimage 110:60–77. https://doi.org/10.1016/j.neuroimage.2015.01.043

Conte S, Richards JE (2021) The influence of the head model conductor on the source localization of auditory evoked potentials. Brain Topogr. https://doi.org/10.1007/s10548-021-00871-z

Conte S, Richards JE (2022) Cortical source analysis of event-related potentials: a developmental approach. Dev. Cogn. Neurosci. 54:101092. https://doi.org/10.1016/j.dcn.2022.101092

Conte S, Richards JE, Guy MW, Xie WZ, Roberts JE (2020) Face-sensitive brain responses in the first year of life. Neuroimage 211:116602. https://doi.org/10.1016/j.neuroimage.2020.116602

de Haan M, Johnson MH, Halit H (2003) Development of face-sensitive event-related potentials during infancy: a review. Int J Psychophysiol 51(1):45–58. https://doi.org/10.1016/S0167-8760(03)00152-1

Deen B, Richardson H, Dilks DD, Takahashi A, Keil B, Wald LL, Saxe R (2017) Organization of high-level visual cortex in human infants. Nat Commun 8(1):1–10

Fillmore PT, Phillips-Meek MC, Richards JE (2015a) Age-specific MRI brain and head templates for healthy adults from 20 through 89 years of age. Front Aging Neurosci 7:44. https://doi.org/10.3389/fnagi.2015.00044

Fillmore PT, Richards JE, Phillips-Meek MC, Cryer A, Stevens M (2015b) Stereotaxic magnetic resonance imaging brain atlases for infants from 3 to 12 months. Dev Neurosci 37(6):515–532. https://doi.org/10.1159/000438749

Fu X, Richards JE (2021) Investigating developmental changes in scalp-to-cortex correspondence using diffuse optical tomography sensitivity in infancy. Neurophotonics 8(3):035003

Gao CJ, Conte S, Richards JE, Xie WZ, Hanayik T (2019) The neural sources of N170: understanding timing of activation in face-selective areas. Psychophysiology 56(6):e13336. https://doi.org/10.1111/psyp.13336

Gilmore JH, Shi F, Woolson SL, Knickmeyer RC, Short SJ, Lin W, Shen D (2011) Longitudinal development of cortical and subcortical gray matter from birth to 2 years. Cereb Cortex 22(11):2478–2485. https://doi.org/10.1093/cercor/bhr327

Gomez J, Barnett MA, Natu V, Mezer A, Palomero-Gallagher N, Weiner KS, Grill-Spector K (2017) Microstructural proliferation

in human cortex is coupled with the development of face processing. Science 355(6320):68–71. https://doi.org/10.1126/science.aag0311

Güllmar D, Haueisen J, Reichenbach JR (2010) Influence of anisotropic electrical conductivity in white matter tissue on the EEG/MEG forward and inverse solution. A high-resolution whole head simulation study. Neuroimage 51(1):145–163. https://doi.org/10.1016/j.neuroimage.2010.02.014

Guy MW, Richards JE, Roberts JE (under review) Corticial source analysis of the face-sensitive N290 component in infants at high risk for autism spectrum disorders

Guy MW, Zieber N, Richards JE (2016) The cortical development of specialized face processing in infancy. Child Dev 87(5):1581–1600. https://doi.org/10.1111/cdev.12543

Guy MW, Richards JE, Tonnsen BL, Roberts JE (2018) Neural correlates of face processing in etiologically-distinct 12-month-old infants at high-risk of autism spectrum disorder. Dev Cogn Neurosci 29:61–71. https://doi.org/10.1016/j.dcn.2017.03.002

Hämäläinen JA, Ortiz-Mantilla S, Benasich AA (2011) Source localization of event-related potentials to pitch change mapped onto age-appropriate MRIs at 6months of age. Neuroimage 54(3):1910–1918. https://doi.org/10.1016/j.neuroimage.2010.10.016

Hansman CF (1966) Growth of interorbital distance and skull thickness as observed in roentgenographic measurements. Radiology 86(1):87–96. https://doi.org/10.1148/86.1.87

Hazlett HC, Gu H, Munsell BC, Kim SH, Styner M, Wolff JJ, Statistical A (2017) Early brain development in infants at high risk for autism spectrum disorder. Nature 542(7641):348–351. https://doi.org/10.1038/nature21369

Hoehl S, Peykarjou S (2012) The early development of face processing—what makes faces special? Neurosci Bull 28(6):765–788

Howell BR, Styner MA, Gao W, Yap P-T, Wang L, Baluyot K, Elison JT (2019) The UNC/UMN Baby Connectome Project (BCP): an overview of the study design and protocol development. Neuroimage 185:891–905. https://doi.org/10.1016/j.neuroimage.2018.03.049

Johnson MH, Griffin R, Csibra G, Halit H, Farroni T, de Haan M, Richards J (2005) The emergence of the social brain network: evidence from typical and atypical development. Dev Psychopathol 17(3):599–619

Lai Y, van Drongelen W, Ding L, Hecox KE, Towle VL, Frim DM, He B (2005) Estimation of in vivo human brain-to-skull conductivity ratio from simultaneous extra- and intra-cranial electrical potential recordings. Clin Neurophysiol 116(2):456–465. https://doi.org/10.1016/j.clinph.2004.08.017

Lew S, Sliva DD, Choe M-S, Grant PE, Okada Y, Wolters CH, Hämäläinen MS (2013) Effects of sutures and fontanels on MEG and EEG source analysis in a realistic infant head model. Neuroimage 76:282–293. https://doi.org/10.1016/j.neuroimage.2013.03.017

Makropoulos A, Aljabar P, Wright R, Hüning B, Merchant N, Arichi T, Rueckert D (2016) Regional growth and atlasing of the developing human brain. Neuroimage 125:456–478. https://doi.org/10.1016/j.neuroimage.2015.10.047

Meijs JW, Weier OW, Peters MJ, Van Oosterom A (1989) On the numerical accuracy of the boundary element method (EEG application). IEEE Trans Biomed Eng 36(10):1038–1049

Michel CM, Brunet D (2019) EEG source imaging: a practical review of the analysis steps. Front Neurol 10(325):00325. https://doi.org/10.3389/fneur.2019.00325

Odabaee M, Tokariev A, Layeghy S, Mesbah M, Colditz PB, Ramon C, Vanhatalo S (2014) Neonatal EEG at scalp is focal and implies high skull conductivity in realistic neonatal head models. Neuroimage 96:73–80. https://doi.org/10.1016/j.neuroimage.2014.04.007

Oostenveld R, Fries P, Maris E, Schoffelen J-M (2011) FieldTrip: open source software for advanced analysis of MEG, EEG, and invasive electrophysiological data. Comput Intell Neurosci

Ortiz-Mantilla S, Hämäläinen JA, Benasich AA (2012) Time course of ERP generators to syllables in infants: a source localization study using age-appropriate brain templates. Neuroimage 59(4):3275–3287. https://doi.org/10.1016/j.neuroimage.2011.11.048

Ortiz-Mantilla S, Hämäläinen JA, Musacchia G, Benasich AA (2013) Enhancement of gamma oscillations indicates preferential processing of native over foreign phonemic contrasts in infants. J Neurosci 33(48):18746. https://doi.org/10.1523/JNEUROSCI.3260-13.2013

Ortiz-Mantilla S, Hämäläinen JA, Realpe-Bonilla T, Benasich AA (2016) Oscillatory dynamics underlying perceptual narrowing of native phoneme mapping from 6 to 12 months of age. J Neurosci 36(48):12095. https://doi.org/10.1523/JNEUROSCI.1162-16.2016

Ortiz-Mantilla S, Realpe-Bonilla T, Benasich AA (2019) Early interactive acoustic experience with non-speech generalizes to speech and confers a syllabic processing advantage at 9 months. Cereb Cortex 29(4):1789–1801. https://doi.org/10.1093/cercor/bhz001

Powell LJ, Kosakowski HL, Saxe R (2018) Social origins of cortical face areas. Trends Cogn Sci 22(9):752–763. https://doi.org/10.1016/j.tics.2018.06.009

Reynolds GD, Richards JE (2005) Familiarization, attention, and recognition memory in infancy: an event-related potential and cortical source localization study. Dev Psychol 41(4):598–615. https://doi.org/10.1037/0012-1649.41.4.598

Reynolds GD, Richards JE (2009) Cortical source localization of infant cognition. Dev Neuropsychol 34(3):312–329. https://doi.org/10.1080/87565640902801890

Richards JE (in prep) Updating the neurodevelopmental MRI database

Richards JE (2005) Localizing cortical sources of event-related potentials in infants' covert orienting. Dev Sci 8(3):255–278. https://doi.org/10.1111/j.1467-7687.2005.00414.x

Richards JE, Conte S (2020) Brain development in infants: structure and experience. In: Tamis-LeMonda C, Lockman JJ (eds) Cambridge handbook of infant development. Cambridge, Cambridge

Richards JE, Xie W (2015) Brains for all the ages: structural neurodevelopment in infants and children from a life-span perspective. In: Bensen J (ed) Advances in Child Development and Behavior, vol 48

Richards JE, Boswell C, Stevens M, Vendemia JM (2015a) Evaluating methods for constructing average high-density electrode positions. Brain Topogr 28(1):70–86. https://doi.org/10.1007/s10548-014-0400-8

Richards JE, Sanchez CE, Phillips-Meek MC, Xie W (2015b) A database of age-appropriate average MRI templates. Neuroimage 124(Pt B):1254–1259. https://doi.org/10.1016/j.neuroimage.2015.04.055

Richards JE, Gao C, Conte S, Guy MW, Xie W (2018). Supplemental information for the neural sources of N170: understanding timing of activation in face-selective areas. https://doi.org/10.13140/RG.2.2.15716.01924

Rosenke M, Weiner KS, Barnett MA, Zilles K, Amunts K, Goebel R, Grill-Spector K (2018) A cross-validated cytoarchitectonic atlas of the human ventral visual stream. Neuroimage 170:257–270. https://doi.org/10.1016/j.neuroimage.2017.02.040

Sanchez CE, Richards JE, Almli CR (2012a) Age-specific MRI templates for pediatric neuroimaging. Dev Neuropsychol 37(5):379–399. https://doi.org/10.1080/87565641.2012.688900

Sanchez CE, Richards JE, Almli CR (2012b) Neurodevelopmental MRI brain templates for children from 2 weeks to 4 years of age (vol 54, pg 77, 2012). Dev Psychobiol 54(4):474–474. https://doi.org/10.1002/dev.21018

Thorpe SG, Cannon EN, Fox NA (2016) Spectral and source structural development of mu and alpha rhythms from infancy through adulthood. Clin Neurophysiol 127(1):254–269. https://doi.org/10.1016/j.clinph.2015.03.004

van der Weel FR, van der Meer AL (2009) Seeing it coming: infants' brain responses to looming danger. Naturwissenschaften 96(12):1385–1391. https://doi.org/10.1007/s00114-009-0585-y

van Leeuwen T, Been P, van Herten M, Zwarts F, Maassen B, van der Leij A (2007) Cortical categorization failure in 2-month-old infants at risk for dyslexia. NeuroReport 18(9):857–861. https://doi.org/10.1097/WNR.0b013e3280c1e2bf

Vorwerk J, Cho J-H, Rampp S, Hamer H, Knösche TR, Wolters CH (2014) A guideline for head volume conductor modeling in EEG and MEG. Neuroimage 100:590–607. https://doi.org/10.1016/j.neuroimage.2014.06.040

Vorwerk J, Oostenveld R, Piastra MC, Magyari L, Wolters CH (2018) The FieldTrip-SimBio pipeline for EEG forward solutions. Biomed Eng 17(1):1–17

Wang Y, Gotman J (2001) The influence of electrode location errors on EEG dipole source localization with a realistic head model. Clin Neurophysiol 112(9):1777–1780. https://doi.org/10.1016/S1388-2457(01)00594-6

Wolters CH, Anwander A, Tricoche X, Weinstein D, Koch MA, MacLeod RS (2006) Influence of tissue conductivity anisotropy on EEG/MEG field and return current computation in a realistic head model: a simulation and visualization study using high-resolution finite element modeling. Neuroimage 30(3):813–826. https://doi.org/10.1016/j.neuroimage.2005.10.014

Xie W, Richards JE (under review) Cortical source analysis in EEG frequency analysis

Xie W, Richards JE (2016) Effects of interstimulus intervals on behavioral, heart rate, and event-related potential indices of infant engagement and sustained attention. Psychophysiology 53(8):1128–1142. https://doi.org/10.1111/psyp.12670

Xie W, Richards JE (2017) The relation between infant covert orienting, sustained attention and brain activity. Brain Topogr 30(2):198–219. https://doi.org/10.1007/s10548-016-0505-3

Xie W, Mallin BM, Richards JE (2019a) Development of brain functional connectivity and its relation to infant sustained attention in the first year of life. Dev Sci 22(1):e12703. https://doi.org/10.1111/desc.12703

Xie W, McCormick SA, Westerlund A, Bowman LC, Nelson CA (2019b) Neural correlates of facial emotion processing in infancy. Dev Sci 22(3):e12758